The Plant Cell, Vol. 32: 1519–1535, May 2020, www.plantcell.org © 2020 ASPB.

SHORTROOT-Mediated Intercellular Signals Coordinate Phloem Development in Arabidopsis Roots[OPEN]

Hyoujin Kim,[a,1] Jing Zhou,[a,b,c,1] Deepak Kumar,[a] Geupil Jang,[a,d] Kook Hui Ryu,[a] Jose Sebastian,[a,b,e] Shunsuke Miyashima,[f] Ykä Helariutta,[f,g] and Ji-Young Lee[a,h,2]

[a] School of Biological Sciences, College of Natural Science, Seoul National University, Seoul 08826, Korea
[b] Boyce Thompson Institute, Cornell University, Ithaca, New York 14853
[c] Elo Life Systems, Durham, North Carolina 27709
[d] School of Biological Sciences and Technology, Chonnam National University, Gwangju 61186, Korea
[e] Department of Biological Sciences, Indian Institute of Science Education and Research, Berhampur 760010, India
[f] Institute of Biotechnology, Department of Biological and Environmental Sciences, University of Helsinki, FIN-00014, Finland
[g] Sainsbury Laboratory, Cambridge University, Bateman Street, Cambridge CB2 1LR, United Kingdom
[h] Plant Genomics and Breeding Institute, Seoul National University, 1 Gwanak-ro, Gwanak-gu, Seoul 08826, Korea

ORCID IDs: 0000-0003-3317-6996 (H.K.); 0000-0002-0252-2588 (J.Z.); 0000-0002-5816-5129 (D.K.); 0000-0001-8637-1782 (G.J.); 0000-0002-0400-4493 (K.H.R.); 0000-0002-1826-0308 (J.S.); 0000-0001-8267-3978 (S.M.); 0000-0002-7287-8459 (Y.H.); 0000-0002-7631-5127 (J.-Y.L.)

Asymmetric cell division (ACD) and positional signals play critical roles in the tissue patterning process. In the Arabidopsis (*Arabidopsis thaliana*) root meristem, two major phloem cell types arise via ACDs of distinct origins: one for companion cells (CCs) and the other for proto- and metaphloem sieve elements (SEs). The molecular mechanisms underlying each of these processes have been reported; however, how these are coordinated has remained elusive. Here, we report a new phloem development process coordinated via the SHORTROOT (SHR) transcription factor in Arabidopsis. The movement of SHR into the endodermis regulates the ACD for CC formation by activating microRNA165/6, while SHR moving into the phloem regulates the ACD generating the two phloem SEs. In the phloem, SHR sequentially activates *NAC-REGULATED SEED MORPHOLOGY 1* (*NARS1*) and *SECONDARY WALL-ASSOCIATED NAC DOMAIN PROTEIN 2* (*SND2*), and these three together form a positive feedforward loop. Under this regulatory scheme, NARS1, generated in the CCs of the root differentiation zone, establishes a top-down signal that drives the ACD for phloem SEs in the meristem. SND2 appears to function downstream to amplify NARS1 via positive feedback. This new regulatory mechanism expands our understanding of the sophisticated vascular tissue patterning processes occurring during postembryonic root development.

INTRODUCTION

The evolutionary success of multicellular organisms raises the key developmental question of how their complex morphogenesis is regulated. Studies have shown that asymmetric cell division (ACD) and positional information play critical roles in the temporal and spatial regulation of tissue patterning during morphogenesis (Berger et al., 1998; Kerszberg and Wolpert, 2007; Abrash and Bergmann, 2009; De Smet and Beeckman, 2011; Kajala et al., 2014). Plant cells, caged in the rigid cell wall, largely rely on direct cell-to-cell communication through plasmodesmata to exchange positional information.

Phloem is a tissue evolved to facilitate long-distance nutrient transport from source to sink. Sieve elements (SEs) and companion cells (CCs) form a functional unit for phloem (reviewed in Oparka and Turgeon, 1999). SEs, enucleated living cells, form tubular networks and serve as a conduit for transporting carbohydrates, amino acids, and minerals as well as RNAs, proteins, and diverse signaling molecules throughout the plant body (Sjolund, 1997; Knoblauch and van Bel, 1998; Hayashi et al., 2000). CCs that develop adjacent to SEs are responsible for the loading of sugars to the SEs through the plasmodesmata (Lohaus et al., 1995). In the Arabidopsis root, phloem is organized in a relatively simple manner and thus serves as a good system for a precise analysis of tissue patterning. Two phloem poles develop perpendicular to the xylem axis in the Arabidopsis root, generating a bisymmetric structure. In each pole, proto- and metaphloem SEs are generated by the ACD of a SE precursor cell and two CCs are generated by ACDs of procambial cells neighboring both the SE precursor and pericycle cells (Figures 1A and 1B; Mähönen et al., 2000).

Recent studies have revealed the molecular components that regulate phloem development (Blob et al., 2018). OCTOPUS (OPS), BREVIS RADIX (BRX), CLAVATA3/ESR-RELATED 45 (CLE45), and SMAX1-LIKE 3-5 (SMXL3-5) are important for both the ACD of phloem SE precursor cells and the differentiation of protophloem SEs (Truernit et al., 2012; Rodriguez-Villalon et al., 2014; Wallner et al., 2017). When these genes are mutated, SE does not differentiate properly, and the ACD of the phloem SE precursor is often missing. This ACD defect was proposed to stem

[1] These authors contributed equally to this work.
[2] Address correspondence to jl924@snu.ac.kr.
The author responsible for the distribution of materials integral to the findings presented in this article in accordance with the policy described in the Instructions for Authors (www.plantcell.org) is Ji-Young Lee (jl924@snu.ac.kr).
[OPEN]Articles can be viewed without a subscription.
www.plantcell.org/cgi/doi/10.1105/tpc.19.00455

IN A NUTSHELL

Background: Phloem is responsible for transporting photosynthetic products and other essential molecules from where they are produced (source) to where they are needed (sink). Phloem consists of sieve elements that act as conduits of molecules and companion cells that supply molecules to sieve elements. As a functional unit of phloem, sieve elements and companion cells should develop in a highly coordinated manner. However, underlying molecular processes have not been identified. The development of both sieve elements and companion cells is severely disrupted in the root meristem when a gene encoding SHORTROOT transcription factor is mutated in *Arabidopsis thaliana*. In the Arabidopsis root, SHORTROOT protein is produced in the xylem side of the stele and then moves to the phloem and the outer cell layer.

Question: We wanted to understand how the development of sieve elements and companion cells is coordinated. To this end, we dissected the phloem development and molecular pathways mediated by SHORTROOT in the root of *Arabidopsis thaliana*.

Findings: We found that SHORTROOT coordinates phloem development via two pathways. One is via the activation of microRNA 165/6 in the outer layer of the root stele. This is required for keeping the level of Homeodomain leucine zipper class III transcription factors under control, thereby maintaining companion cell development. The other involves the sequential activation of *NAC-REGULATED SEED MORPHOLOGY 1* (*NARS1*) and *SECONDARY WALL-ASSOCIATED NAC DOMAIN PROTEIN 2* (*SND2*), encoding NAC domain transcription factors, in the phloem. Under this regulatory scheme, NARS1 is generated in the companion cells of the root differentiation zone, and then establishes a top-down signal that drives the development of sieve elements in the meristem. SND2 appears to function downstream of NARS1 and amplify *NARS1* expression via positive feedback regulation. This novel regulatory mechanism expands our understanding of the sophisticated tissue patterning processes during root growth and development.

Next steps: Phloem plays critical roles in allocating resources in plant bodies. Understanding the design principles of phloem development could facilitate engineering crops with better yields.

from perturbations in rootward signals that are transmitted through differentiated phloem SE (Rodriguez-Villalon et al., 2014). Among these signals, one is thought to be auxin transported by PIN proteins through the phloem SE. Proper PIN localization on the SE membrane was shown to be controlled by BRX and PROTEIN KINASE ASSOCIATED WITH BRX (PAX; Marhava et al., 2018). Several transcription factors (TFs) are also involved in the phloem development process. *ALTERED PHLOEM DEVELOPMENT* (*APL*) encoding a MYB TF regulates the differentiation of phloem and xylem vessels. PHLOEM EARLY DOF (PEAR) TFs act as short-distance mobile signals that control ACD in the phloem pole through antagonistic interactions with Homeobox-leucine zipper (HD-ZIP) III TFs in the xylem and procambium (Bonke et al., 2003; Miyashima et al., 2019). In addition, multiple NAC-domain TFs were found to regulate the specifications and differentiation of protophloem SE (Furuta et al., 2014; Kondo et al., 2016). These findings indicate that phloem development is achieved via complex regulatory programs that involve local and long-distance signals. However, it is unclear how ACDs for SE and CC development are coordinated in space and time.

Here, we report that the SHORTROOT (SHR) coordinates ACDs for CC and SE development. *SHR* mRNA is transcribed in parts of the stele, that is, the xylem, procambium, and pericycle cells neighboring the xylem and procambium. Subsequently, SHR proteins actively move into the phloem pole, the remaining pericycle cells, the endodermis, and the QC (Supplemental Figures 1F and 1G; Helariutta et al., 2000; Nakajima et al., 2001; Sena et al., 2004). From the endodermis, SHR controls the ACD for CC; from the phloem, it directs the ACD for SE development by directly regulating NARS1, a NAC-domain TF.

RESULTS

SHR Is Required for Phloem Development

To determine whether SHR is involved in phloem development, we examined the phloem morphology in *shr-2* roots. In addition to the xylem patterning defects reported previously (Carlsbecker et al., 2010), we found severe disruption in the phloem development process. In the wild-type Arabidopsis root, the xylem axis is composed of a row of cells made of protoxylem and metaxylem (Figure 1A). Perpendicular to the xylem axis, two poles of phloem tissues are established. In contrast to the wild type, where two SEs develop, in *shr-2* roots, we observed one SE-like cell in a phloem pole (Figures 1B and 1C). To examine SEs more accurately, we performed two experiments. First, we visualized callose localized onto sieve plates on phloem SEs by staining with aniline blue. In the wild type, two sieve plates on neighboring strands were observed (Supplemental Figure 1A). However, in *shr-2*, only one sieve plate was detected (Supplemental Figure 1B). Second, we used immunohistochemistry to locate early SE nodulin-like proteins (SE-ENOD) that specifically accumulate in differentiating SE (Khan et al., 2007). This experiment allowed a quantitative analysis of the distribution of SEs in each root. Consistent with the aniline blue staining results, we detected SE-ENOD in both proto- and metaphloem SEs in the maturation zone of wild-type roots (Figure 1D; Supplemental Figure 2A). However, in *shr-2* roots, we observed variations in the SE development process and therefore classified them into the following six groups: class 1 as a group without any SE, class 2 with SE found only in one phloem pole, class 3 with one SE in each of the two phloem poles, class 4 with

more than one SE in one pole and one SE in the other, class 5 with two SEs in each of the two phloem poles, and class 6 with more than two SEs in one phloem pole and two SEs in the other. SEs belonging to class 5 in *shr* roots were aligned laterally neighboring the pericycle, whereas those in wild-type roots were always aligned perpendicular to the xylem axis. Approximately 75% of *shr-2* roots developed SEs belonging to classes 1 to 4, further supporting a reduction in SEs (Figure 1E; Supplemental Figure 2A). We also simplified this classification by simply counting the number of phloem SEs (Supplemental Figure 2B; Supplemental Data Set 1A). This analysis further supports the significant reduction of phloem SEs in *shr-2* in comparison with the wild type [$P \leq 0.0001$; one-way ANOVA followed by Dunnett's multiple comparisons test ($\alpha = 0.05$)].

We then examined the expression patterns of phloem markers in the wild-type and *shr-2* roots. A previous lineage analysis of vascular cells in the Arabidopsis root showed that proto- and metaphloem SEs in one phloem pole are generated from sequential ACDs of a SE procambium precursor and a SE precursor and that two CCs are generated by ACDs of two procambium cells neighboring both a SE precursor and the pericycle (Mähönen et al, 2000; Bonke et al., 2003). *ProAPL:*endoplasmic reticulum-localized GFP (*erGFP*) expression starts in the developing protophloem SEs in the meristem (Figure 1F) and then switches to the developing CCs and metaphloem SEs when the protophloem SEs mature (Figure 1J; Bonke et al., 2003). Expression of *ProAPL:erGFP* in *shr-2* starts not in the meristem but in the elongation zone, suggesting a delay in phloem differentiation in comparison to neighboring cell types (Figure 1G; Carlsbecker et al., 2010). In *shr-2*, GFP expression of *ProAPL:erGFP* was first observed in a single SE-like cell, after which the expression expanded asymmetrically to only one of its neighboring cells, which becomes CC (Figure 1K). We also examined the status of CC by analyzing the expression of *ProSUC2:erGFP*, which is specifically expressed in CCs in the mature part of the root (Figures 1H and 1L; Stadler and Sauer, 1996). Unlike in wild-type roots, *ProSUC2:erGFP* in *shr-2* was expressed sporadically only in one cell next to the SE (Figures 1I and 1M), consistent with the expansion of *ProAPL:erGFP* to only one cell neighboring a SE. Taken together, our data suggest that when the SHR function is lost, the cell division activities required for the formation of both CCs and SEs are compromised.

The SHR-SCR-miR165/6 Pathway Regulates Procambial Cell Division

SHR in the endodermis and quiescent center (QC) activates and interacts with SCARECROW (SCR), another GRAS-family TF, and together they activate the expression of *microRNA165*/166 (*miR165/6*) to pattern xylem vessels. *MiR165/6*, produced in the endodermis, helps to establish the *HD-ZIP III* gradient in the stele, which subsequently specifies metaxylem in the center and protoxylem in the periphery of the stele in a dosage-dependent manner (Carlsbecker et al., 2010; Miyashima et al., 2011).

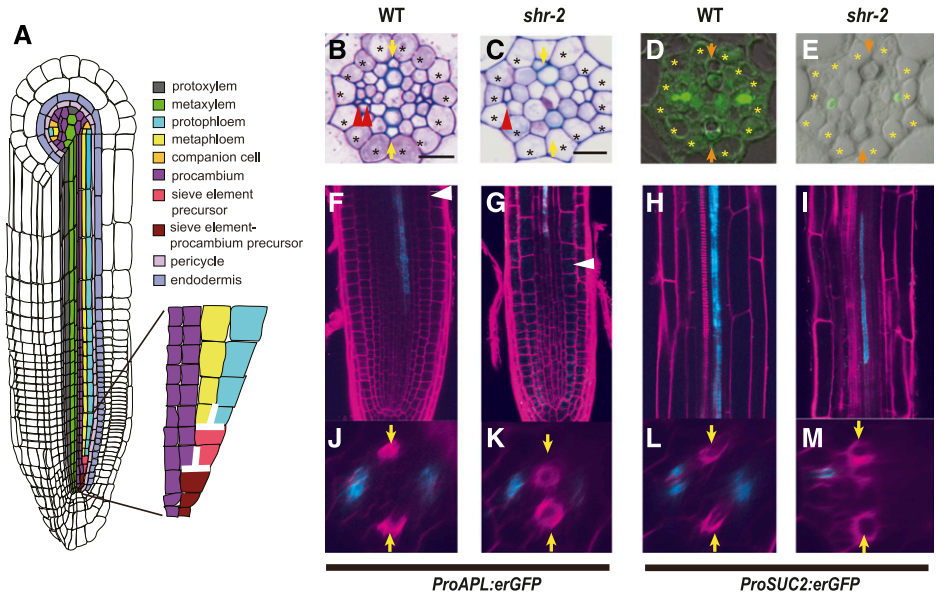

Figure 1. SHR Regulates Phloem Development in the Arabidopsis Root.

(A) A schematic diagram showing the Arabidopsis root anatomy and asymmetric cell divisions of two precursor cells for phloem sieve element formation, as indicated by the flipped T shape in white. Comparison of phloem development between wild-type and *shr-2* roots.

(B) and **(C)** Transverse sections through the maturation zones of wild-type **(B)** and *shr-2* **(C)** roots, stained with toluidine blue. Scale bar = 10 μm. Asterisks, pericycle position; arrows, xylem axis; red arrowheads, sieve elements. WT, wild type.

(D) and **(E)** Immunolocalization of the SE-ENOD in wild-type **(D)** and *shr-2* **(E)** roots. Asterisks, pericycle position; arrows, xylem axis. WT, wild type.

(F) to **(M)** Expression of of two representative phloem markers. *ProAPL:erGFP* in the wild type (**[F]** and **[J]**) and *shr-2* (**[G]** and **[K]**), and expression of *ProSUC2:erGFP* in wild type (**[H]** and **[L]**) and *shr-2* (**[I]** and **[M]**). Arrows, xylem axis; red arrowheads, sieve elements; white arrowheads, beginning of the transition zone of the root. WT, wild type.

To test whether the SHR-SCR-miR165/6 pathway also influences other aspects in the stele besides xylem development, we examined the stele cell organization and phloem development characteristics in the *ProUAS:MIR165A shr-2 J0571* line that drives *miR165* expression in the ground tissue of the *shr* mutant (Carlsbecker et al., 2010). In this line, we observed a stochastic recovery of stele cell numbers in some individuals (Figure 2A; Supplemental Figure 2C). These recovered cells appeared to be mostly procambial cells between xylem and phloem poles. Consistent with this, *shr-2 phb-6*, a double mutant between *SHR* and *PHABULOSA* (*PHB*), showed a significant recovery of the procambial cell number (Figure 2B; Supplemental Figure 2C; Supplemental Data Set 1B). Nevertheless, our histological analyses indicated that phloem SEs did not recover in either of these two lines (Figures 2A, 2B, 2E, and 2F; Supplemental Figures 2A and 2B). Instead, these lines suggest an increase in CC cell numbers, as indicated by the expansion of the *ProSUC2:erGFP* expression level (more than two cells that surround a SE demonstrated evidence of expression) in *shr-2 phb-6* (Supplemental Figure 3D).

SCR interacts with SHR in the endodermis to produce *miR165/6*. Hence, *scr-4*, the loss-of-function mutant, displayed evidence of disruption of cell proliferation activity and xylem patterning, similar to *shr-2*. Although *scr-4* showed a reduction in the number of procambial cells, similar to that of *shr*, it constantly showed two SEs in at least one of the two phloem poles (Figures 2C and 2G). A similar case was also observed when we examined the SEs in transgenic plants harboring *ProCRE1:PHBem-GFP*, which expresses a microRNA-resistant version of *PHB*, under the promoter of the stele-specific gene *CRE1* (Sebastian et al., 2015). This line overexpresses functional PHB throughout the stele, as in the *shr* mutant. Similar to *shr-2*, roots expressing *ProCRE1:PHBem-GFP* exhibited a significant reduction in the procambium cell number (Figure 2D; Supplemental Figure 2C; Supplemental Table 3B). However, the average number of SEs in the roots expressing *ProCRE1:PHBem-GFP* did not differ significantly from that in wild-type roots (Figure 2H; Supplemental Figures 2A and 2B). These data suggest that the primary role of the bidirectional signaling pathway, which involves SHR, SCR, miR165/6 and PHB, may be to control procambial cell proliferation, including ACD for CCs, rather than ACD for SE formation.

In the wild-type Arabidopsis root meristem, *PHB* is transcribed throughout the stele; however, its mRNA and protein are excluded from the stele periphery (Carlsbecker et al., 2010). We thus asked whether the exclusion of PHB from the phloem precursors is important for proper procambium cell proliferation. To address this, we introduced microRNA-resistant *PHB* (*PHBm*) fused to GFP under the protophloem- and phloem precursor-specific *S32* promoter (*AT2G18380*) into *shr-2 phb-6* (Lee et al., 2006). Indeed, the *ProS32:PHBm-GFP shr-2 phb-6* line showed a reduction in the number of procambium cells (Supplemental Figures 3A to C). These data confirm that for procambium cell proliferation, *PHB* mRNAs should be actively excluded from phloem precursors via the SHR-SCR-miR165/6 pathway.

SHR Moving into the Phloem Pole Promotes Cell Division for Phloem Sieve Element Formation

Given that bidirectional signaling does not account for the formation of the two SEs, we asked whether SHR in the stele promotes this process. To address this, we expressed *SHR* exclusively in the root stele in *shr-2* plants. We did this by expressing a nonmobile version of SHR, *SHRΔNLELDV*, which was fused to GFP with a nuclear localization signal, under the *CRE1* promoter (Figure 3A; Supplemental Figure 4A; Mähönen et al, 2000; Carlsbecker et al., 2010). *SHRΔNLELDV* does not have cell-to-cell mobility but still retains its biological function (Gallagher and Benfey, 2009). In *ProCRE1:SHRΔNLELDV-nlsGFP shr-2*, we observed partial recovery of the root growth (Supplemental Figure 4C). Consistent with earlier findings (Carlsbecker et al.,

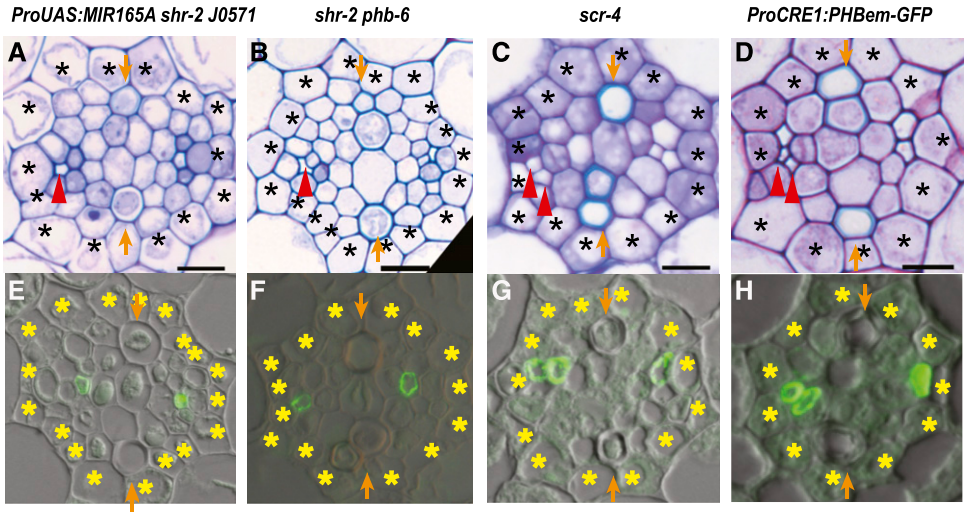

Figure 2. PHABULOSA Suppresses Procambial Cell Divisions for Companion Cell Development.

Toluidine blue–stained transverse sections and immunolabeled SE-ENOD of *ProUAS:MIR165A shr J0571* (**[A]** and **[E]**), *shr-2 phb-6* (**[B]** and **[F]**), *scr-4* (**[C]** and **[G]**) and *ProCRE1:PHBem-GFP* (**[D]** and **[H]**) are shown. Scale bar = 10 μm; asterisks, pericycle position; arrows, xylem axis; arrow heads, SEs.

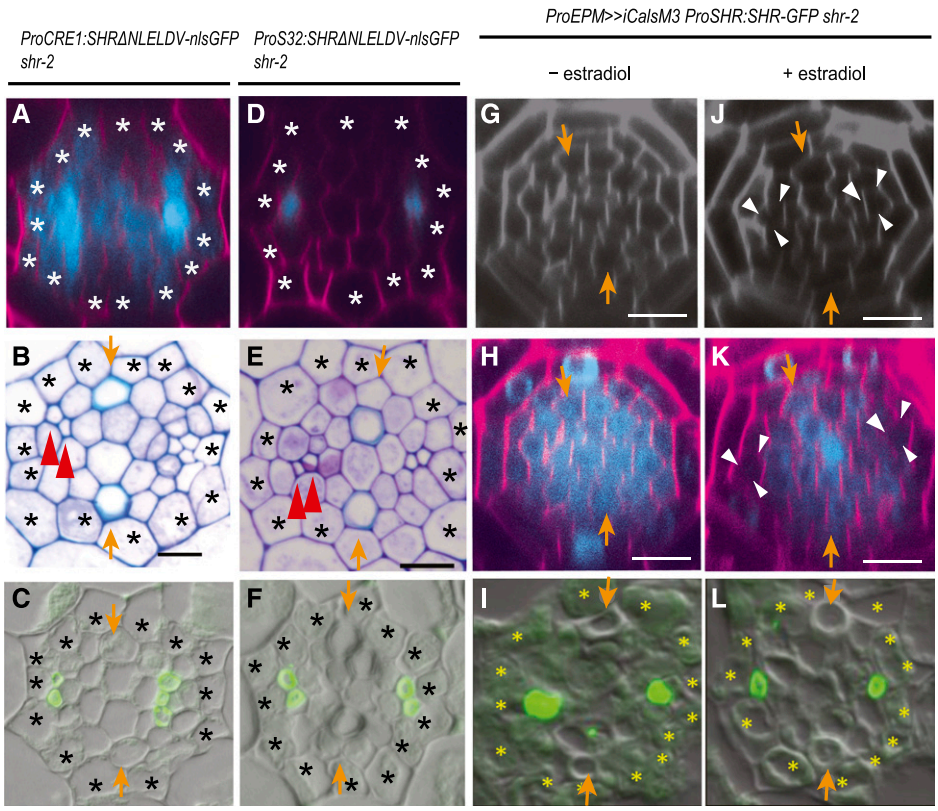

Figure 3. SHR Movement into the Phloem Pole Is Required for Asymmetric Cell Divisions for Sieve Element Development.

(A) to **(L)** Confocal cross sections of the root meristematic zone of *ProCRE1:SHRΔNLELDV-nlsGFP shr-2* **(A)** and *ProS32:SHRΔNLELDV-nlsGFP shr-2* **(D)** show the GFP signal indicating the expression pattern of the nonmobile SHR protein. Toluidine blue–stained transverse sections and immunolocalization of the SE-ENOD of *ProCRE1:SHRΔNLELDV-nlsGFP shr-2* (**[B]** and **[C]**) and *ProS32:SHRΔNLELDV-nlsGFP shr-2* (**[E]** and **[F]**) are shown. Confocal cross sections of the root meristematic zone and immunolocalization of the SE-ENOD of *ProEPM>>iCalsM3 ProSHR:SHR-GFP shr-2* (**[G]** to **[L]**) are also shown.
(G) to **(I)** Without an estradiol treatment, SHR movement and SE development are normal.
(J) to **(L)** Images taken 2 d after a treatment with 10 μM of estradiol. The phloem pole, indicated by white arrowheads, does not show SHR-GFP. Scale bar = 10 μm; asterisks, pericycle position; arrows, xylem axis; arrowheads, SEs.

2010), xylem patterning was not restored in this transgenic line (Supplemental Figure 4B). However, both a histological analysis and the immunolocalization of SE-ENOD demonstrated an increase in the SE number but not in procambial cells (Figures 3B and 3C; Supplemental Figures 2A to 2C), strongly indicating that SHR in the stele specifically promotes ACD for SE formation.

In the root meristem, *SHR* is transcribed in the xylem and procambium but not in the phloem pole cells. However, subsequently the SHR protein moves into phloem poles. We thus asked whether the movement of SHR into the phloem is required for ACD and the subsequent formation of SEs. To address this, we expressed *SHRΔNLELDV* in the phloem in the *shr-2* background using the *S32* promoter (Figure 3D). The expression of *ProS32:SHRΔNLELDV-nlsGFP* did not significantly mitigate the stele cell proliferation defect in *shr-2* (Figure 3E). However, we found that two SEs develop in *ProS32:SHRΔNLELDV-nlsGFP shr-2* (Figure 3F). These results suggest that SHR proteins moving into the phloem pole in the root meristem promote ACD for SE formation.

To corroborate our findings, we created an experimental context in which SHR cannot move into the phloem pole cells. It was previously shown that excessive callose accumulation at the plasmodesmata can block SHR movement (Vatén et al., 2011). Consistent with this, when we expressed a gain-of-function mutant of *CALLOSE SYNTHASE 3* (*CAL3-M*) under the EPM (S29) promoter with estradiol-mediated induction (Lee et al., 2006; Miyashima et al., 2019), SHR failed to move into the SE initially (Figures 3G, 3H, 3J, and 3K). We analyzed the status of phloem SE development in these transgenic lines further and observed the formation of only one SE when CAL3-M was induced in the phloem pole (Figures 3I and 3L). Taken together, our results suggest that SHR moving into the phloem pole promotes cell division for the formation of the phloem sieve element.

NARS1-SND2 Form a Downstream Pathway of SHR in the Phloem

SHR moving into the phloem pole likely regulates the expression of other TFs specifically in the phloem to drive ACD for the formation

of two SEs in the root meristem. To identify these downstream candidate TFs, we analyzed high-resolution, cell type-specific gene expression data of Arabidopsis roots (Nawy et al., 2005; Lee et al., 2006; Levesque et al., 2006; Brady et al., 2007; Carlsbecker et al., 2010). First, we selected 1089 phloem-enriched genes from cell type-specific data using the criteria of at least threefold enrichment in phloem cell types and corrected p-values < 0.001 (Figure 4A).

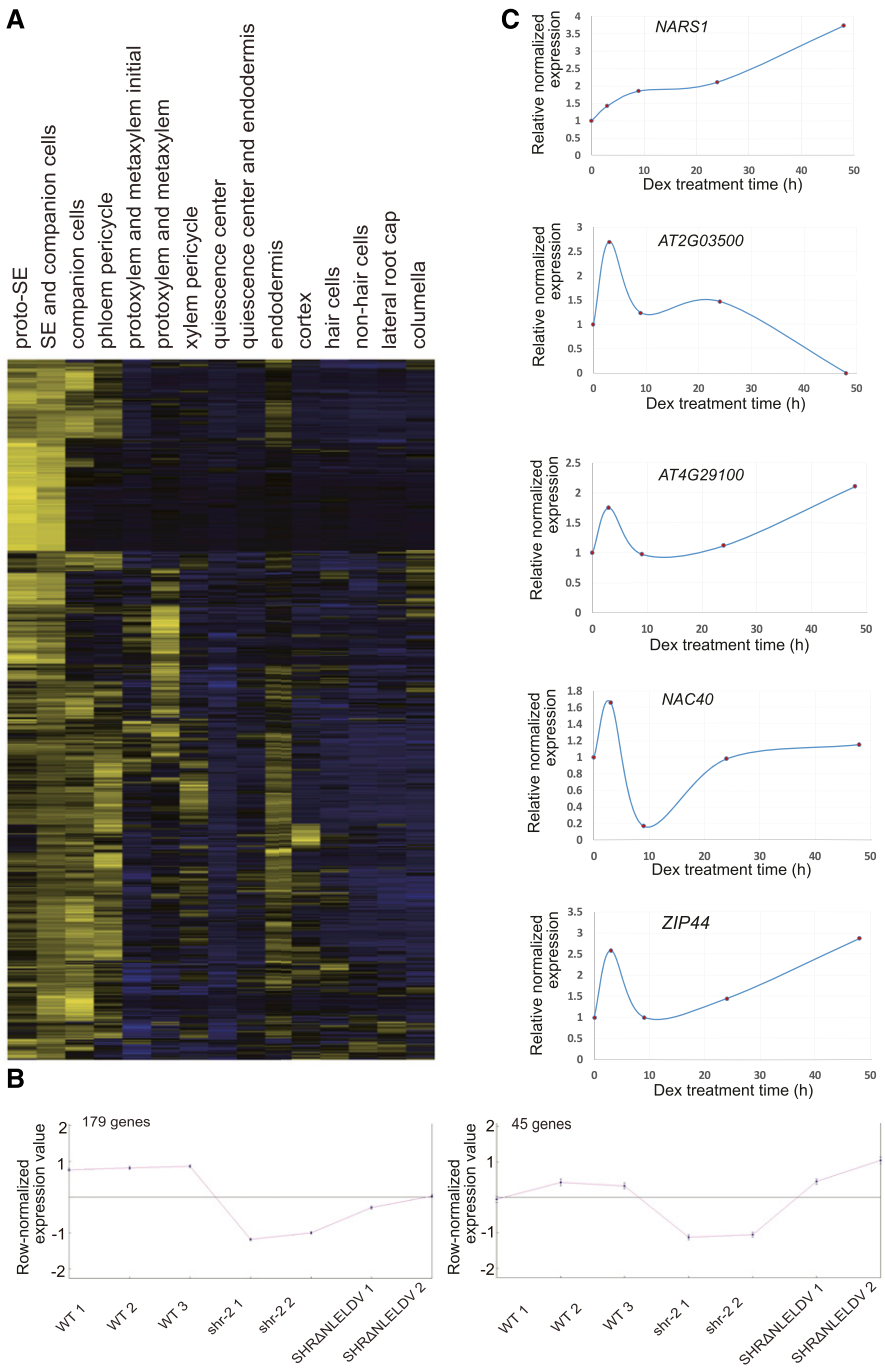

Figure 4. Genome-Wide Meta-Analysis and Time-Course Induction Experiments Identify Phloem-Enriched Transcription Factors Downstream of SHR.

(A) Root expression of genes that are enriched in the phloem cell types.
(B) Centroid graphs of two QT clusters for which phloem-enriched genes under the regulation of SHR in the stele were identified.
(C) Time-course expression changes of putative direct target genes of SHR in the *ProSHR:SHR-GR shr-2* line in response to different Dex treatment durations.

Next, we generated genome-wide gene expression data for a meta-analysis, as follows. *ProCRE1:erGFP* was introduced into wild-type and *shr-2* backgrounds to express GFP in the stele cells of the root meristem. We then collected GFP-expressing stele cells from the wild type, *shr-2* and *ProCRE1:SHRΔNLELDV-nlsGFP shr-2,* through fluorescence activated cell sorting. RNAs were extracted from the sorted cells of each line and processed to generate labeled probes to be hybridized onto a GeneChip Arabidopsis Tiling 1.0R Array (Affymetrix). Normalized expression data are available in Supplemental Data Set 2. We then examined the influence of SHR on 1089 phloem-enriched genes in the tiling array data. Because our meta-analysis was performed with phloem-enriched genes, we only considered those that are up-regulated by SHR. To find them, we clustered the expressions of the 1089 phloem-enriched genes in the wild type, *shr-2* and *ProCRE1:SHRΔNLELDV-nlsGFP shr-2* (Heyer et al., 1999). This analysis revealed two clusters consisting of 224 genes that are down-regulated in *shr-2* in comparison to the wild type, with the expression then restored in *ProCRE1:SHRΔNLELDV-nlsGFP shr-2* (Figure 4B; Supplemental Data Set 3). This list of genes included 24 TFs.

To search for potential direct targets of SHR among the 24 TFs, we micro-dissected and extracted the RNAs from the roots of *ProSHR:SHR-GR shr-2* upon induction with dexamethasone (Dex) in a time series and then measured the expression changes of candidate TFs by means of digital droplet (DD) RT-PCR (Supplemental Figure 5; Taylor et al., 2017). Like SCR, a confirmed direct target of SHR (Levesque et al., 2006), five TFs showed an increase in their expression level in response to SHR induction (Figure 4C).

NARS1 (*NAC-REGULATED SEED MORPHOLOGY 1*; *ANAC056*; *AT3G15510*) encoding the NAC-domain TF has been shown to regulate the development and degeneration of integuments during embryogenesis (Kunieda et al., 2008). Given that it shows quick and steady induction in response to SHR, we conducted a closer examination of its potential involvement in SE development together with another gene encoding NAC-domain TF, *SND2* (*SECONDARY WALL-ASSOCIATED NAC DOMAIN PROTEIN 2*; *ANAC073*; *AT4G28500*), a slower responder to SHR induction than *NARS1* (Supplemental Figure 5; Zhong et al., 2007). We performed chromatin immunoprecipitation (ChIP) followed by real-time qPCR using *pSHR*::*SHR:GFP shr-2* roots to establish whether SHR-GFP directly binds to the NARS1 promoter (Figure 5A). In three repeated experiments, we consistently identified binding of SHR-GFP to the ~1-kb and ~3-kb upstream regions of the *NARS1* translation start site. We also analyzed the expression domains of *NARS1* in transcriptional and translational reporter fusion lines in wild-type and *shr-2* plants (Figure 5B). *ProNARS1:erGFP* in the wild type showed expression in the CCs of the differentiation zone in the root. However, we could not detect GFP signals from the transgenic lines expressing *ProNARS1:GFP-NARS1* (data not shown). In *shr-2*, no evidence of the transcriptional or translational fusion GFP of *NARS1* was detected (Figure 5B). These data collectively suggested *NARS1* as a direct downstream target of SHR.

Despite the fact that *SND2* was induced much later than *NARS1* by SHR, its expression in the root was detected in the meristem (Figure 5C). An analysis of *pSND2*::*β-glucuronidase* (*GUS*) plants revealed that *SND2* is expressed in the protophloem SEs of the meristem zone and metaxylem of the maturation zone. The expression pattern of the SND2 protein in the transgenic lines expressing *ProSND2*:*SND2-GFP* was identical to that of the transcriptional fusion line. Transcriptional and translational expression patterns of *SND2* were also examined in *shr* plants. Interestingly, all of the aforementioned phloem-associated expression instances disappeared, and only the metaxylem-specific expression of *SND2* was retained in *shr-2*, suggesting that SND2 is a part of the SHR regulatory program responsible for phloem development.

NARS1 Regulates Asymmetric Cell Divisions of Sieve Element Precursors

The possible involvement of *SND2* and *NARS1* in the phloem development process was investigated in more depth using T-DNA/transposon insertion lines of these genes (CS124048, *snd2-1*; *SALK_137131*; *nars1-2*). In s*nd2-1*, a Spm transposable element is inserted in the second exon of the coding region and in *nars1-2*, a T-DNA is inserted at the 3′ untranslated region (Supplemental Figures 6A and 6C support Figures 6 and 7). RT-qPCR indicated that the *snd2-1* and *nars1-2* lines are likely null mutants (Supplemental Figures 6B and 6D support Figures 6 and 7). In an analysis of the root lengths, the roots of *nars1-2* were found to be significantly shorter than those of the wild type (Supplemental Figure 6E). These two mutant lines were used in the rest of this study without allele numbers unless otherwise indicated.

We examined phloem phenotypes in *snd2* and *nars1* by introducing phloem markers. A CC status analysis based on *ProAPL:erGFP* indicated that CC development is normal in these mutants (Supplemental Figures 7A to 7C support Figures 6 and 7). We also asked whether NARS1 and SND2 participate in the SE differentiation program directed by NAC45/86, regulating the enucleation process of protophloem SEs (Furuta et al., 2014). An expression analysis of *ProNAC45:GUS-GFP* in the wild type, *snd2*, and *nars1* indicated no change in *NAC45* expression levels at the protophloem SE position (Supplemental Figures 7D to 7I support Figures 6 and 7). Consistent with this, we did not detect any gap cell in either of these mutants, which indicates a defect in the differentiation of protophloem SEs (Figures 6A to 6C; Truernit et al., 2012).

Linking H2B to GFP makes GFP very stable (Mähönen et al., 2014). When we examined a potential defect in the enucleation process of *snd2* and *nars1* mutants by analyzing the expression of a differentiating protophloem marker, *ProAT5G48060:H2B-YFP* (Figures 6D to 6F), we found something unexpected. Unlike the wild type and *snd2*, *nars1* plants expressing *ProAT5G48060:H2B-YFP* exhibited H2B-YFP not only in the phloem SE but also in the cells neighboring phloem SEs, as denoted by the yellow arrows in Figures 6D to 6F. Nevertheless, enucleation was consistently observed as the SE cells started to undergo elongation in all of the genotypes, suggesting no defects during protophloem differentiation (bottom panels in Figures 6D to 6F). Thus, we also explored the phloem SE lineage by analyzing the expression of two independent transgenic lines of *ProS32:H2B-GFP nars1*. In those lines, we found multiple stele cell files expressing H2B-GFP

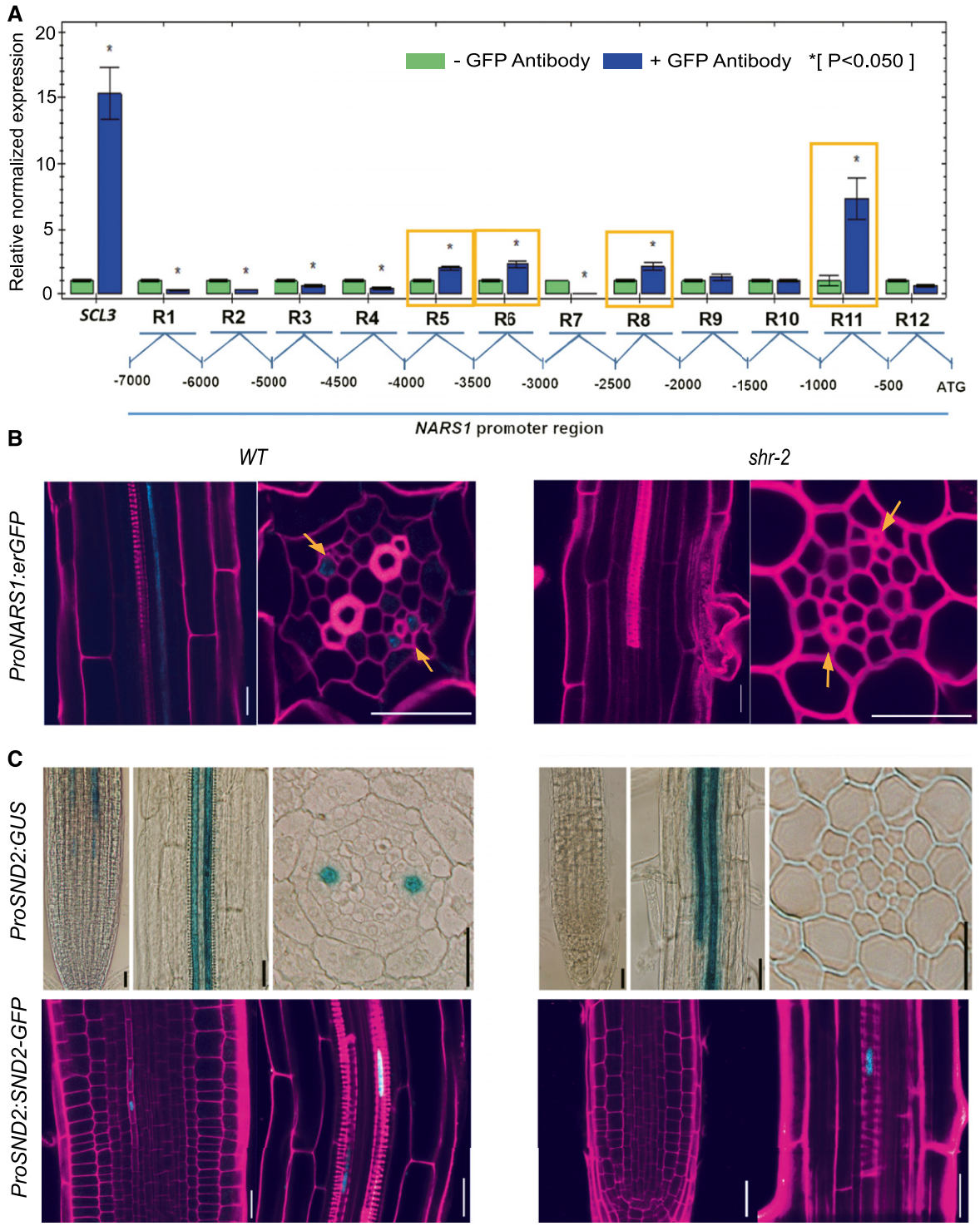

Figure 5. SHR Regulates *NARS1* and *SND2* Expression in the Phloem.

(A) ChIP real-time qPCR analysis for testing the direct binding of SHR to the *NARS1* promoter. A ChIP was performed in roots of 5-DAT *ProSHR:SHR-GFP shr-2* seedlings. *SCL3* is a positive control.

(B) Expression pattern of *NARS1* in the wild type (WT) Col-0 (left) and *shr-2* (right).

(C) Expression pattern of *SND2* in the wild type Col-0 (left) and *shr-2* (right). The transcriptional expression pattern of *SND2* was visualized with the GUS system (*ProSND2:GUS*). The expression of the translational GFP fusion system, *ProSND2:SND2-GFP*, shows a pattern identical to that of transcriptional fusion in the wild type. Scale bar = 20 μm.

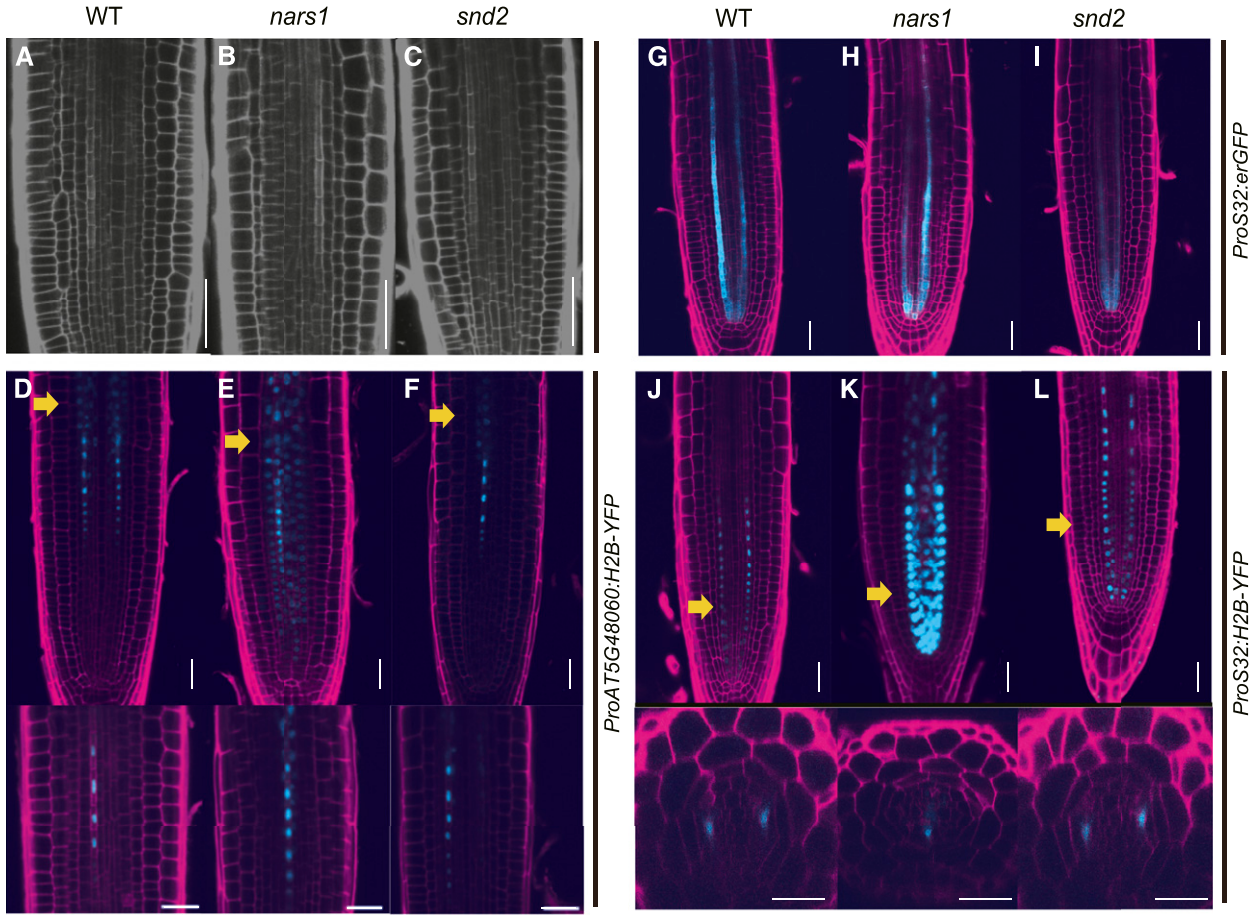

Figure 6. Analysis of Protophloem Lineage and Differentiation in the Wild Type, *nars1*, and *snd2*.

(A) to **(C)** Protophloem differentiation in the root meristem, visualized by propidium iodide staining of the wild type (WT) **(A)**, *nars1* **(B)**, and *snd2* **(C)**.
(D) to **(F)** Nucleus morphologies in the protophloem cell files, visualized with *ProAT5G48060:H2B-YFP* for the WT **(D)**, *nars1* **(E)**, and *snd2* **(F)**. The elongating protophloem undergoing nuclear lysis is marked by the yellow arrow (top) and is magnified (bottom). No noticeable difference in the timing of nuclear lysis is found.
(G) to **(I)** *ProS32:erGFP* expressed in WT **(G)**, *nars1* **(H)**, and *snd2* **(I)**.
(J) to **(L)** Cell lineage analysis of the phloem pole using H2B-YFP expressed under the S32 promoter in the WT **(J)**, *nars1* **(K)**, and *snd2* **(L)**. H2B-GFP is found broadly in the meristem zone of *nars1*, indicating a change in the division patterns of cells in the early phloem lineage. Cross sections of meristems of three genotypes on the regions marked with yellow arrows (bottom). Scale bar = 20 μm.

(Figures 6J to 6L). This phenomenon was not due to the misexpression of *S32* itself given that the expression pattern of *ProS32:erGFP* was not affected in *nars1* (Figures 6G to 6I). *ProS32:erGFP* begins to undergo GFP expression broadly in the procambial cell right above the QC and is then restricted to the phloem precursors and protophloem SE. In *ProS32:H2B-GFP,* stable H2B-GFP would be transferred along the cell lineage as the cells divide. Thus, it may be that the change in the division patterns of the procambial cells in *nars1* resulted in the spread of H2B-GFP to the inner part of the phloem pole.

We then examined phloem cell lineages in *nars1* in comparison with the wild type and *snd2*. Figure 7 shows serial cross sections of the root meristems of the wild type, *nars1*, and *snd2*. Phloem SE precursors that normally divide into two in the wild type (as denoted by the red box in Figures 7A and 7B) did not divide in *nars1* (marked with * in Figures 7E and 7F). Instead, we noticed a division of a procambial cell inside the SE precursor, which normally does not divide (as indicated by the yellow box in Figures 7E and 7F). The lack of SE precursor cell division was further confirmed by optical sections of propidium iodide–stained roots using confocal microscopy (Figures 7Q to 7S). This abnormal cell division in *nars1* led to one SE missing in 8 out of 14 individuals analyzed here by means of SE-ENOD immunolocalization, making its SE number significantly lower than that of the wild type [$P \leq 0.001$; one-way ANOVA followed by Dunnett's multiple comparisons test ($\alpha = 0.05$); Figure 7H; Supplemental Figures 2A and 2B; Supplemental Data Set 1A]. Consistent with these findings, *nars1-1*, SM_3_28017, also displayed defects during the ACD of the phloem SE precursor and during SE differentiation (Supplemental Figure 6F). By contrast, the *snd2* mutant did not show any defect during the

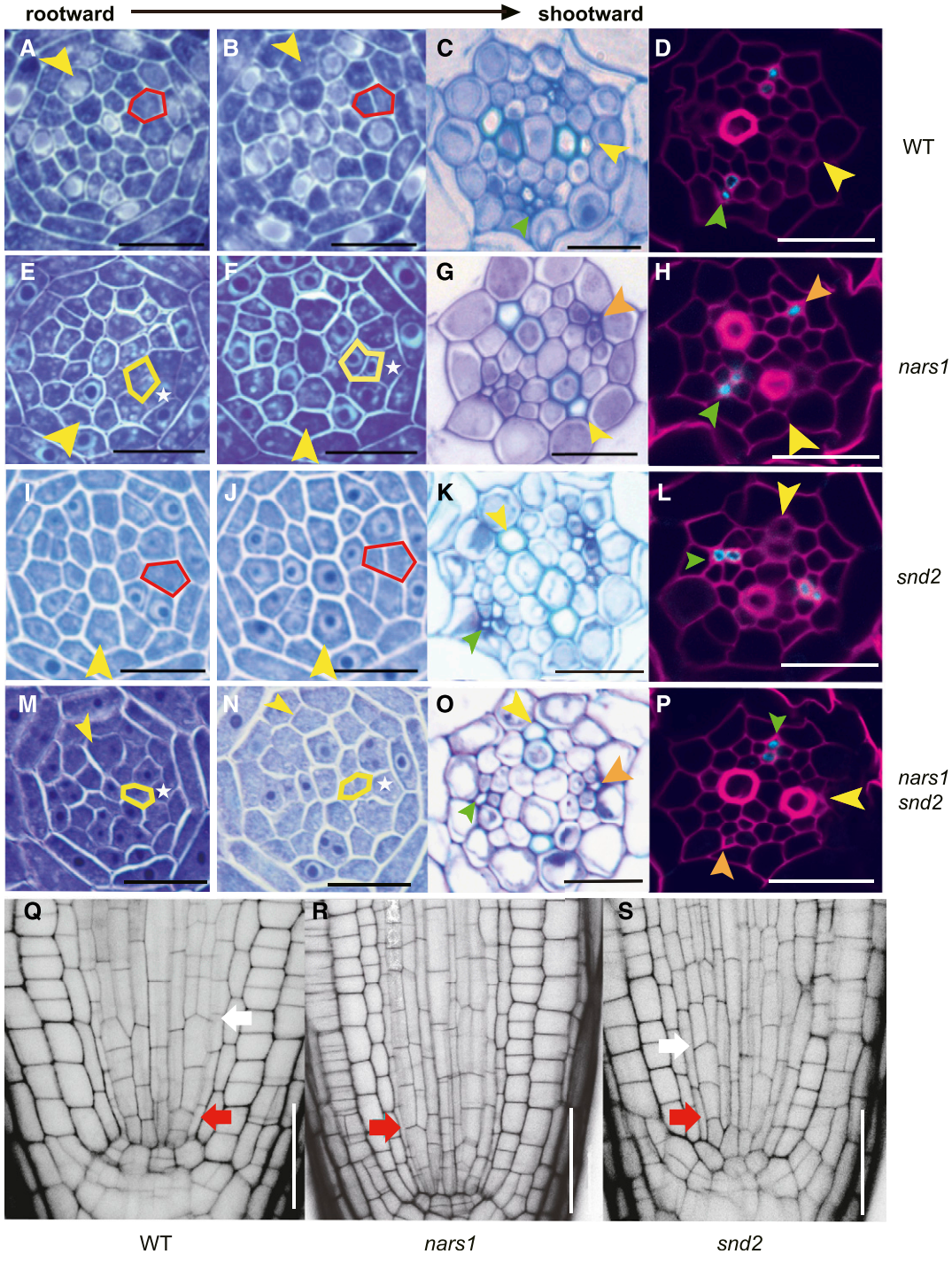

Figure 7. Analysis of Cell Division Patterns for Phloem Sieve Element Development in the Wild Type, *nars1* and *snd2*.

(A) to **(P)** Analysis of division patterns of phloem SE precursors in the roots of the wild type (WT; **[A]** to **[D]**), *nars1* (**[E]** to **[H]**), *snd2* (**[I]** and **[L]**) and the *nars1 snd2* double mutant (**[M]** to **[P]**). Analysis of cell division patterns using consecutive cross-sections in WT (**[A]** and **[B]**), *nars1* (**[E]** and **[F]**), *snd2* (**[I]** and **[J]**) and *snd2 nars1* double mutant (**[M]** and **[N]**) and resulting cell organization in the root differentiation zone (**[C], [G], [K]** and **[O]**). SE-ENOD immunolocalization shows two differentiated phloem SEs in WT **(D)** and *snd2* **(L)** but only one in *nars1* **(H)** and *nars1 snd2* **(P)**.

(Q) to **(S)** Confocal images of wild-type **(Q)**, *nars1* **(R)**, and *snd2* **(S)** root meristems. Phloem precursor cells in the wild type and *snd2* divide twice, whereas that in *nars1* divides only once. Yellow arrowhead, xylem axis; green arrowhead, pole with two phloem SEs; orange arrowhead, pole with one phloem SE; red arrow, ACD of the procambium-phloem initial; white arrow, ACD of the phloem SE initial; Scale bar = 20 μm.

division of SE precursors (Figures 7I to 7L; Supplemental Figures 2A and 2B). Combining these data, we conclude that NARS1 is responsible for the ACD of the phloem SE precursor as a downstream target of SHR.

NARS1 Functions as a Potential Top-Down Signal

NARS1 regulates the ACD of the SE precursor in the root meristem despite the fact that it is expressed in the CCs of the root differentiation zone (Figures 5 and 7). By contrast, SND2 expressed in the protophloem SE of the root meristem does not influence the division process. To gain a deeper understanding of the regulatory relationships between the two, we introduced *ProNARS1:erGFP* into *snd2* and *ProSND2:GUS* into *nars1*. Analyses of marker gene expression levels indicated that NARS1 promotes *SND2* expression in the protophloem as an upstream regulator (Supplemental Figure 8). Consistent with this relationship, the *nars1 snd2* double mutant did not show any additive phenotype (Figures 7M to 7P). SE-ENOD immunolocalization also demonstrated that *nars1 snd2* had a defect in the number of differentiated SEs (6 out of 20 individuals).

We then asked how NARS1 produced in the CCs of the root differentiation zone can act during the ACD of the SE precursors. To visualize NARS1 translationally fused with GFP, we chose N-terminal tagged GFP because we failed to detect a GFP signal when we expressed GFP fused to the C terminus of NARS1, even under the CRE1 promoter (see below). Unfortunately, GFP fused to NARS1 during translational fusion under the *NARS1* promoter was undetectable. Thus, we expressed GFP-NARS1 under two strong phloem specific promoters, S29 and SUC2, in the *nars1* background (Figures 8A to 8E). The *S29* (*PEAR1*, *AT2G37590*) promoter drives the expression in the phloem precursors of the root meristem (Lee et al., 2006), and *SUC2* drives the expression in the CCs of the root differentiation zone, slightly earlier than the *NARS1* promoter (Supplemental Figure 9C). We detected nuclear-localized GFP-NARS1 expression under the S29 promoter in phloem precursors (Figure 8A). In *ProSUC2:GFP-NARS1 nars1* plants, however, we did not find GFP in the CC, instead finding punctate fluorescence in the stele (Figures 8B and 8C). Nevertheless, both lines showed full recovery of the SE precursor division in the meristem (14 observed for *ProS29:GFP-NARS1*; 21 observed for *ProSUC2:GFP-NARS1*; Figures 8A and 8B) and root growth ($P < 0.001$ according to a Student's *t* test; Figures 8D and 8E).

Taken together, these data indicate that NARS1, generated in the CCs of the differentiation zone, functions as a top-down signal, either as a mobile factor itself or as a trigger of another mobile signal that locally regulates the ACD of SE precursors (Figure 8N). Because GFP-NARS1 in *ProSUC2:GFP-NARS1 nars1* could not be visually inspected, we tested this hypothesis indirectly by analyzing the influence of NARS1 on the expression of SHR-downstream TFs in the phloem. Specifically, we micro-dissected 1-mm-long root tips of *nars1*, *ProSUC2:GFP-NARS1 nars1* and *ProS29:GFP-NARS1 nars1* so that we could exclude most regions where the *SUC2* promoter drives *NARS1* expression, after which we extracted small amounts of RNA for each genotype. Then, using Droplet Digital RT-PCR (DD-PCR), we quantified and compared the transcript levels of SHR-downstream phloem TFs in *ProSUC2:GFP-NARS1 nars1* and *ProS29:GFP-NARS1 nars1* against those in *nars1*. In this analysis, 17 out of 24 SHR-downstream phloem TFs were up-regulated in *ProSUC2:GFP-NARS1 nars1*, and only six of these were also up-regulated in *ProS29:GFP-NARS1 nars1* (Supplemental Figure 9A). Interestingly, *SND2* was induced only in *ProSUC2:GFP-NARS1 nars1* but not in *ProS29:GFP-NARS1 nars1*. Furthermore, the expression domain of 17 downstream TFs in the cell-type-specific root expression data indicated that TFs up-regulated by *ProSUC2:GFP-NARS1* are not limited to the phloem starting in the root differentiation zone (Supplemental Figure 9B). Taken together, NARS1 expressed in the CC appears to facilitate its control of phloem-enriched TFs within a broad range.

Positive Feedforward Loop in Action for Phloem Sieve Element Development

The significance of NARS1 with regard to SE development was further addressed by analyzing the SE status using SE-ENOD immunolocalization in transgenic roots expressing *NARS1* throughout the stele under the *CRE1* promoter. Five out of 22 transgenic plants with *ProCRE1:GFP-NARS1* showed more than two SEs in each phloem pole (Figures 8F to 8H). Furthermore, *ProCRE1:GFP-NARS1* in *shr-2* resulted in the significant restoration of the SE number (Figures 8L and 8M; Supplemental Figures 2A and 2B). Interestingly, *SND2* expressed under the *CRE1* promoter also showed an increase in phloem SEs (6 out of 27; Figures 8I to 8K). Consistent with the SE-ENOD immunolocalization outcome, we observed the expansion of the *ProAPL:erGFP* domain in roots expressing *ProCRE1:SND2* and *ProCRE1:NARS1* (Supplemental Figure 10). However, *ProSUC2:erGFP* was not affected by ectopic *SND2* or *NARS1* expression (Supplemental Figure 11).

The *snd2* mutant does not affect the SE number despite the fact that ectopically expressed SND2 can do so. Thus, we asked whether such a phenomenon occurs because SND2 can amplify *NARS1* expression via positive feedback regulation. Indeed, we found upregulation of *NARS1* transcript by threefold in roots expressing *ProCRE1:SND2-GFP* in comparison to non-transgenic Col-0 roots (Supplemental Figure 12B). In addition, ChIP followed by real-time qPCR of *ProSHR:SHR-GFP* roots against the upstream intergenic region of *SND2* indicated the binding of SHR to the *SND2* promoter (Supplemental Figure 12C). Our time-course analysis of *ProSHR:SHR-GR* demonstrated the induction of *SND2* at a time point much later than that of *NARS1.* Thus, this result indicates that SHR directly regulates SND2 expression in the presence of other SHR-dependent component(s).

Lastly, we asked whether the *NARS1* pathway is affected when CC development is perturbed via the SHR-SCR-miR165/6 pathway. We examined this by measuring *NARS1* and *SND2* in *scr-4* and *ProCRE1:PHBem-GFP* roots (Supplemental Figure 12A). Indeed, their expression levels were significantly reduced in both of these genetic backgrounds. Together, these results indicate that while the ACD of a SE precursor is primarily via the direct regulation of *NARS1* by SHR in the root stele, it partly depends on proper CC development as mediated via SHR in the endodermis.

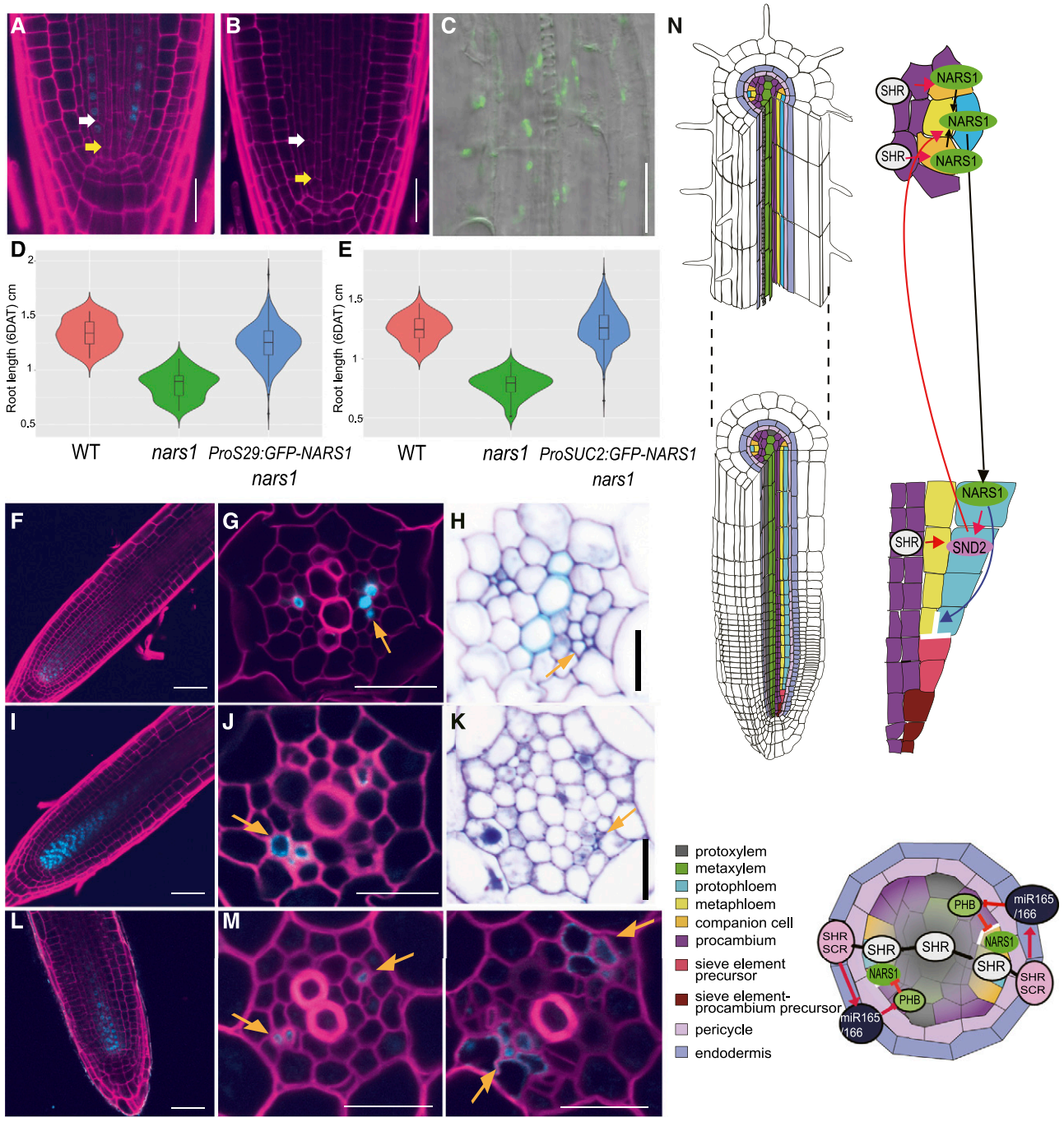

Figure 8. Functional Analysis of NARS1 as a Potential Top-Down Signal for Asymmetric Cell Divisions of Sieve Element Precursors and a Proposed Molecular Model.

(A) to **(C)** Analysis of the division recovery of phloem SE precursors in the roots of *ProS29:GFP-NARS1 nars1* **(A)** and *ProSUC2:GFP-NARS1 nars1* (**[B]** and **[C]**).

(D) and **(E)** Analysis of the root length recovery process of *ProS29:GFP-NARS1 nars1* [three independent homozygous T3 lines ($n = 263$), wild type (WT; $n = 32$) and *nars1* ($n = 50$); **(D)**] and *ProSUC2:GFP-NARS1 nars1* (three independent homozygous T3 lines [$n = 256$], WT [$n = 35$] and *nars1* [$n = 50$]; **[E]**).

(F) to **(H)** Transgenic roots expressing *ProCRE1:GFP-NARS1* Col-0.

(I) to **(K)** Transgenic roots expressing *ProCRE1:SND2-GFP* Col-0.

(L) and **(M)** Transgenic roots expressing *ProCRE1:GFP-NARS1 shr-2*. Longitudinal views of the root meristem expressing GFP-NARS1 **(F, L)** and SND2-GFP **(I)** are shown.

(G), **(J)**, and **(M)** SE-ENOD immunolocalization.

DISCUSSION

In the Arabidopsis root, phloem SEs and CCs are generated by the ACDs of different precursors rather than a single precursor (Baum et al., 2002; Bonke et al., 2003). However, their development is highly coordinated. In this study, we report how such coordination is achieved via SHR movements. SHR that moves into the phloem pole is primarily responsible for the ACD of the SE precursor, while SHR moving into the endodermis is responsible for the ACD of the procambium neighboring SE precursor and pericycle, which generates the CC and procambium.

Using a combination of approaches, including genome-wide expression in the root stele, time-course induction, and ChIP experiments, we identified a detailed pathway led by SHR. ChIP experiments showed that SHR can bind to both the *NARS1* and *SND2* promoters. However, time-course induction analyses indicated that SHR-GR activates *NARS1* shortly after induction (three hours post Dex treatment), whereas for *SND2* this occurs at a much later time point (24 h post Dex treatment). Thus, SND2 induction by SHR appears to require other SHR-dependent components. Combining these results with genetic analyses, we conclude that SHR, NARS1, and SND2 form a positive feedforward loop (Figure 8N). In this regulatory scheme, *NARS1* is likely critical for the ACDs of SE precursors for the following reasons: first, the *nars1* mutant fails to undergo ACD of the SE precursors with frequent reductions in the SE number, and second, the ectopic expression of *NARS1* throughout the stele can increase the degree of SE formation, even in the *shr* mutant. Although the effects of the ectopic expression of *SND2* are similar to those associated with *NARS1*, this appears to occur through the activation of *NARS1* via positive feedback regulation. The induction of *NARS1* in the line ectopically expressing *SND2* throughout the stele supports this idea.

Usually, developmental regulatory pathways are explained in terms of the temporal order of cell type formation and differentiation. By contrast, *NARS1* expressed in the phloem CC of the root differentiation zone activates *SND2* expression in the protophloem SE of the meristem, as well as 16 other phloem-enriched TFs out of the 24 phloem-enriched SHR-downstream TFs. Furthermore, NARS1 is critical for the division of the SE precursor in the meristem. Nonetheless, the artificial expression of *NARS1* in phloem precursors under the *S29* promoter can sufficiently offset ACD defects in *nars1*, suggesting that NARS1 acts locally for ACD. These findings indicate that NARS1 has the potential to serve as a top-down mobile signal to instruct the ACD for phloem SE formation (Figure 8N). However, this aspect requires additional investigations because we could not visualize the NARS1 protein on the move.

The SHR-NARS1 pathway is also important for root growth. In *nars1* or *shr*, root growth is reduced (Supplemental Figure 6E). *ProS32:SHRΔNLELDV-nlsGFP shr-2* transgenic plants, which show restoration of the SE number, also show significantly recovered root growth (Supplemental Figure 4C). *NARS1* expressed either in the phloem precursor or in the CC in the *nars1* mutant also showed restored root growth (Figures 8D and 8E). Taken together, fully functional SEs appear to be critical for root growth, which has also been indicated in other mutants with defects in phloem differentiation (Ingram et al., 2011; Rodriguez-Villalon et al., 2014; Wallner et al., 2017; Blob et al., 2018).

Distinctive from SHR moving to the phloem pole, SHR moving into the endodermis controls the division of procambial cells, including CC formation. In this case, *miR165/6* generated in the endodermis is likely required to suppress the *PHB* level in the phloem pole, which otherwise would inhibit the procambial cell division for CC development (Figure 8N; Supplemental Figure 3). A recent study showed that HD-ZIP III TFs suppress the expression of *PEAR* (*PHLOEM EARLY DOF*) genes, whose proteins generated in the protophloem SE move to procambial cells to promote cell divisions of lateral neighbors of the protophloem SE (Miyashima et al., 2019). Our stele profiling data detected only minor recoveries of *DOF6* and *OBP2* in *ProCRE1:SHRΔNLELDV-nlsGFP shr-2* (Supplemental Data Set 2), supporting the hypothesis that SHR in the endodermis, not in the stele, is primarily responsible for *PEAR* expression. Nevertheless, the status of CC appears partly to influence SE development. Roots expressing miRNA-resistant *PHB* and *scr* roots show down-regulation of *NARS1* and *SND2* and display fewer SEs (Supplemental Figures 2A and 12A). Considering that the CC is the component that unloads transported materials to the SE, such a coordinated reduction of CC and SE would preserve resources. How such communications are achieved at the molecular level would be an interesting topic to explore.

In summary, we report a new aspect of phloem development in Arabidopsis roots. There are many reports describing the regulation of phloem development in Arabidopsis roots. However, earlier studies have been restricted to the development of either SEs or CCs. Our finding that SHR coordinates two ACDs for phloem tissue patterning through the generation of both local and potentially long-distance top-down signals highlights how sophisticated the vascular tissue patterning in the root is. Although seemingly counter-intuitive, the generation of a remote signal initiated by NARS1 in the root differentiation zone via SHR may be a strategy to ensure phloem formation during indeterminate root growth. The subsequent activation of *SND2* by *SHR* and *NARS1* and the amplification of *NARS1* by *SND2* via positive feedback regulation may enhance the robustness of this process (Figure 8N;

Figure 8. (continued).

(H) and **(K)** Toluidine blue staining.

(N) Proposed model of phloem development initiated by *SHR* in Arabidopsis roots. The regulatory scheme shown on the longitudinal axis illustrates the positive feedforward regulatory loop composed of *SHR*, *NARS1*, and *SND2* and the positive feedback regulation between *NARS1* and *SND2*. In the cross section, the repression of *NARS1* by *PHB* is shown. Red arrow, gene regulation; black arrow, intercellular movement. In **(A)** and **(B)**, yellow arrows indicate the ACDs of procambium-phloem SE precursors, and white arrows indicate the ACDs of phloem SE precursors. Orange arrows in **(G)**, **(H)**, **(J)**, **(K)**, and **(M)** indicate ectopic phloem SEs. Scale bar = 20 μm.

Mangan and Alon, 2003). Further studies on how NARS1 regulates the ACDs of SE precursors and a systems approach to the newly identified regulatory motif could deepen our understanding of this key tissue patterning process in vascular plants.

METHODS

Plant Materials and Growth Conditions

Arabidopsis (*Arabidopsis thaliana*) ecotype Columbia (Col-0) was used. Seeds were surface-sterilized, plated (1× Murashige and Skoog [MS] medium with 1% [w/v] Suc), and grown under a 16-h–light/8-h–dark cycle at 22° to 23°C in a plant growth chamber. Light was provided with fluorescence lamps (Kumho, Korea) with a light intensity of 100 μmol m^{-2} s^{-1}. *nars1-2* (SALK_137131) and *snd2-1* (CS124048) were obtained from the Arabidopsis Biological Resources Center (ABRC). Primers used for PCR-based genotyping are listed in Supplemental Data Set 4. The following marker lines were described previously: *ProNAC45:GUS-GFP* (Furuta et al., 2014), *ProAPL:erGFP* (Bonke et al., 2003), and *ProSUC2:erGFP* (Stadler and Sauer, 1996).

Plasmid Construction

Gateway cloning technology (Invitrogen) was used for DNA manipulations. The methods used for the generation of the *S29*, *S32*, and *CRE1* promoters in pDONR P4_P1R was previously described by Lee et al. (2006) and Carlsbecker et al. (2010). *PHB* cDNA was cloned into pDONR221 and mutagenized to *PHBm* as previously described by Carlsbecker et al. (2010). *SHRΔNLELDV* was amplified from the plasmid containing *SHRΔNLELDV* and cloned into pDONR221 (Gallagher and Benfey, 2009). *GFP:nosT* and *nlsGFP* for C terminus translational fusion were cloned into pDONR P2R_P3 by means of BP recombination. *ProS32:PHBm-GFP* was constructed into dpGreen-Bar by Multisite Gateway LR recombination. *pCRE1*::*SHRΔNLELDV:nlsGFP* and *ProS32:SHRΔNLELDV-nlsGFP* were constructed into dpGreen-BarT, which is the dpGreen-Bar vector with the terminator attached.

The *NARS1* and *SND2* promoter regions were amplified from Arabidopsis Col-0 genomic DNA by PCR and inserted into pDONR P4_P1R via a BP reaction. *SND2* cDNA was amplified by RT-PCR and then cloned into pDONR221, and *NARS1* cDNA was cloned into both pDONR221 and pDONR P2R_P3 by a BP reaction. Other components, in this case *GFP*, *GUS*, and *erGFP*, were cloned into pDONR221 and pDONR P2R_P3 by a BP reaction. *ProSND2:SND2-erGFP* and *ProSND2:GUS* were constructed into dpGreen-KanT, and *ProCRE1:SND2*, *ProCRE1:SND2-GFP*, *ProCRE1:NARS1*, *ProCRE1:GFP-NARS1*, *ProS29:GFP-NARS1 ProNARS1:erGFP*, and *ProNARS1:GFP-NARS1* were constructed into dpGreen-BarT by means of Multisite Gateway LR recombination. All clones in the binary vector were transformed into Agrobacterium GV3101 with pSOUP for Arabidopsis transformation by floral dipping (Clough and Bent, 1998).

Confocal Microscopy

All seedling samples were collected at 5 to 6 d after transfer to the growth chamber (DAT). Confocal images were obtained using an LSM700 laser scanning confocal microscope (Zeiss), a TCS SP5 laser scanning confocal microscope (Leica), and a TCS SP8 microscope (Leica) with preset emission/excitation wavelengths of 488 nm/505 to 530 nm for GFP or Alexa Fluor 488, and 561 nm/591 to 635 nm for propidium iodide.

GUS Staining Analysis, Embedding, and Sectioning

The 6-DAT seedlings were incubated in GUS staining solution (100 mM $NaPO_4$ [pH 7.0], 1 mM 5-bromo-4-chloro-3-indolyl-glucuronide, 0.5 mM potassium ferricyanide, and 0.2% [v/v] Triton X-100) at 37°C for 8 h. The samples were then washed with 100 mM $NaPO_4$ (pH 7.0) and incubated in 70% (v/v) ethanol for 1 d at 4°C. For transverse sectioning, Arabidopsis roots were fixed in PBS buffer containing 4% (w/v) paraformaldehyde for 2 h at room temperature. The samples were then dehydrated in a graded series of ethanol (25, 50, 75, and 100% [v/v] in PBS buffer) for 1 h. The dehydrated samples were sequentially incubated in a series of Technovit 8100 cold-polymerizing resin (33, 66, and 100% [v/v] in ethanol) for 3 h each. Sections (3 μm) were taken from the solidified samples with a sectioning machine (RM2255, Leica). For Toluidine blue staining, sections were stained with 0.05% (w/v) Toluidine blue (pH 4.4). Images were imaged with an Axioimager M1 (Zeiss).

Immunostaining of Sieve-Element–Specific SE-ENOD

Two approaches for tissue preparation were utilized in these experiments. One tissue preparation method was performed as described previously using seedlings collected at 5 or 6 DAT (Paciorek et al., 2006). The primary antibody SE-ENOD (Khan et al., 2007) was diluted at a ratio of 1:100 into a blocking solution and incubated for 1.5 h at 37°C. The secondary antibody Alexa Fluor 488 F(ab')2 Fragment of Goat Anti-Mouse IgG, IgM (H+L; cat no. A-11001, Thermo Fisher Scientific) was diluted at a ratio of 1:200 in a blocking solution and incubated for 1 h at room temperature. The microscope slides were mounted with antifadent AF1 (Citifluor) and examined under a laser scanning confocal microscope with an emission/excitation wavelength of 488 nm/505 to 530 nm.

The other tissue preparation method involved sectioning 5- to 6-DAT seedling roots using a vibratome (Leica VT1000S). Seedlings were sectioned after fixing them for 20 min in 4% (w/v) paraformaldehyde dissolved in 1× PBS. The root sections were incubated for 30 min at room temperature in a blocking solution (2% [w/v] of BSA; Sigma-Aldrich) dissolved in 1× PBS). The primary antibody SE-ENOD (early nodulin [ENOD]-like protein 9; AT3G20570; Anti-Phloem Sieve Element [RS6] antibody, cat. no. EIW201, Kerafast) was diluted at a ratio of 1:100 into a blocking solution and incubated overnight at 4°C. The secondary antibody Alexa Fluor 488 F(ab') 2 Fragment of Goat Anti-Mouse IgG, IgM (H+L; cat no. A-11001, Life Technologies) was diluted at a ratio of 1:200 in a blocking solution and incubated for 1 h at room temperature. The root sections were placed on slide glasses, stained with Calcofluor white 2MR (Sigma-Aldrich), and imaged under an LSM700 laser scanning confocal microscope (Zeiss) with emission/excitation wavelengths of 488 nm/505 to 530 nm for Alexa Fluor 488 and 349 nm/420 nm for Calcofluor white 2MR.

For estradiol-induced callose synthesis, seedlings were grown for 3 d on regular MS media and then transferred to MS supplemented with 10 μM of estradiol. Immunolocalization and confocal imaging were performed in 2 d after the estradiol treatment.

Microarray Experiments

All seedling samples were collected at 6 DAT, and the bottom halves of the roots were cut and harvested. Protoplast preparation and fluorescence activated cell sorting facilitated cell sorting were done as described (Birnbaum et al., 2005). Total RNA was isolated using the RNeasy Plant Mini Kit (Qiagen). RNA integrity was determined on a bioanalyzer (Agilent BioAnalyzer 2100). Probe preparation was performed according to the manufacturer's instructions (GeneChip Whole Transcript Double-Stranded Target Assay Manual from Affymetrix Inc.), after which biotinylated double-stranded DNA probes were hybridized to Arabidopsis Tiling 1.0R arrays (Affymetrix). Two to three biological replicates were generated.

Microarray Analysis

To isolate the genes involved in the phloem regulatory networks, we compared gene expression data among phloem SE (S32), SE and

companion cells (APL), companion cells (SUC2), the phloem pole pericycle (S17), protoxylem and metaxylem initials (S4), the protoxylem and metaxylem (S18), the xylem pericycle (J0121), the quiescence center (AGL42), the quiescence center and endodermis (scr5), the endodermis (E30), the cortex (CORTEX), hair cells (COBL9), non-hair cells (gl2), the lateral root cap (LRC), and columella (pet111; Nawy et al., 2005; Lee et al., 2006; Levesque et al., 2006; Brady et al., 2007; Carlsbecker et al., 2010) using the LIMMA package (Smyth, 2004). We identified 1089 genes that are enriched in S32 and/or the APL cell file (fold enrichment >3; corrected p-value < 0.001).

Microarray data from the tiling 1.0R array CDF that contains gene-specific single-copy exonic probe sets were normalized using the RMA algorithm in BIOCONDUCTOR (Irizarry et al., 2003; Naouar et al., 2009). High-correlation coefficients were confirmed within biological replicate data. The aforementioned 1089 phloem-enriched genes were then examined with regard to their expression levels in the wild type, *shr-2*, and *ProCRE1:SHRΔNLELDV-nlsGFP shr-2*. Quality threshold (QT) clustering of differentially expressed genes was performed, and the results were visualized using MultiExperiment Viewer (Saeed et al., 2006).

RT-qPCR Analysis

To analyze the expression level of *SND2* in *snd2* mutant plants, RT-qPCR analyses were performed using total RNAs extracted from 7-DAT root tissues in Col-0, *snd2*, *nars1* plants. Total RNA extraction was performed with a RNeasy plant mini-prep kit according to the manufacturer's instructions (Qiagen). A 20-μL reverse-transcript reaction was conducted for the first cDNA strand synthesis using 1 μg of total RNAs and Superscript III reverse transcriptase (Invitrogen). After the completion of the reverse-transcription reaction, the cDNA template was diluted fivefold by adding 80 μL of double distilled water, and 1 μL of cDNA template was used for a 10-μL qPCR reaction. For the qPCR reactions, a master mix was prepared using iQTM SYBR Green Supermix (Bio-Rad) and a PCR reaction and fluorescence detection were performed using a CFX96 real-time PCR machine (Bio-Rad). GAPDH was used as an internal control gene for this analysis. Primer sequences are provided in Supplemental Data Set 4.

DD-PCR Analysis

To quantify the expression changes of the 24 TFs downstream of SHR in the *NARS1* complementation lines, seeds of *nars1, ProSUC2:GFP-NARS1 nars1*, and *ProS29:GFP-NARS1 nars1* were germinated and grown on MS agar media with 1% (w/v) Suc for 5 d. Segments of root tips ~1 mm long were dissected and collected from each genotype, and the total RNA was then isolated from these using RNeasy Plant Mini Kits (QIAGEN). Here, 0.3 μg of total RNA was used for RT with SuperScript III reverse transcriptase (Invitrogen), as described above.

To quantify the expression of the phloem-enriched SHR-regulated TFs in response to the active form of SHR, 4-d-old seedlings of *SHR:SHR-GR shr-2* were treated with 10 μM of dexamethasone. Total RNA was isolated from different root samples treated with dexamethasone for 0 h, 3 h, 9 h, 24 h, and 48 h. DD-PCR was performed as per the method described below. The GR gene was used as a loading control.

Each 20-μL DD-PCR reaction mixture contained 1× EvaGreen ddPCR Supermix (Bio-Rad), gene-specific primers (Supplemental Data Se 4), and 2.5 μL of the cDNA sample (4 ng). Then 70 μL of Droplet Generation Oil (Bio-Rad) was mixed into each reaction mixture so that 20 μL of the DD-PCR reaction mixture could be segregated into 14,000 ~17,000 droplets using a QX200 droplet generator (Bio-Rad). All droplets, at ~40 μL, were transferred to 96-well plates (Bio-Rad). The PCR steps were performed in a T100 thermal cycler (Bio-Rad) with the following cycling conditions: one cycle at 94°C for 3 min, 40 cycles of 94°C for 30 s, 61°C for 45 s, and 72°C for 60 s, and followed by one cycle of 4°C for 5 min and 90°C for 5 min. The ramping rate was set to 2°C/s throughout the cycles. After PCR was complete, the fluorescence intensity of the droplets was measured with a QX200 droplet reader (Bio-Rad). With QuantaSoft droplet reader software (Bio-Rad), both positive and negative droplet populations were detected and a data analysis was conducted. Via the Poisson statistics, the target mRNA concentrations were determined, with background-correction performed based on nontemplate control data. The absolute transcript levels were calculated in copies/μl of the PCR reaction mixture.

ChIP Analysis

Amounts of 1.3 mg of root samples were collected from 5-DAT *ProSHR:SHR-GFP shr-2* plants for a ChIP analysis. These samples were fixed in PBS buffer containing 1% (v/v) formaldehyde and 5 mM EDTA for 10 min at room temperature. After fixation and upon the addition of 2.5 M Gly solution and then washing twice with PBS containing 5 mM EDTA, the samples were ground in liquid nitrogen and resuspended in an extraction solution (50 mM Tris-HCl, pH 7.5; 150 mM NaCl; 1% [v/v] Triton X-100; 0.1% [w/v] sodium deoxycholate; 2.5 mM EDTA; 10% [v/v] glycerol, supplemented with a 1× protease inhibitor cocktail [Sigma] and 1 mM phenylmethylsulfonyl fluoride [Sigma]). Sonication was performed eight times each for 5 s at 35% to 40% amplitude (Branson Sonifier 250D). GFP antibody (ab290, Abcam) and Protein A agarose (Upstate) underwent precipitation at 4°C overnight. After wash with a low-salt washing buffer, a high-salt washing buffer, and a LiCl washing buffer (low-salt washing buffer 150 mM NaCl, 0.2% [w/v] SDS, 0.5% [v/v] Triton X-100, 2 mM EDTA, and 20 mM Tris-HCl, pH 8; high-salt washing buffer: 500 mM NaCl, 0.2% [w/v] SDS, 0.5% [v/v] Triton X-100, 2 mM EDTA, and 20 mM Tris-HCl, pH 8; LiCl washing buffer: 0.25 M LiCl, 0.5% [v/v] Nonidet P-40, 0.5% [w/v] sodium deoxycholate, 1 mM EDTA, 10 mM Tris-HCl, pH 8), DNA was collected by ethanol precipitation. The *NARS1* and *SND2* promoter enrichment outcome was analyzed by qPCR using a master mix, which was prepared using iQTM SYBR Green Supermix (Bio-Rad). PCR reaction and fluorescence detection were performed using a CFX96 real-time PCR machine (Bio-Rad) with the following conditions: one cycle at 94°C for 3 min, 39 cycles of 94°C for 30 s, 57°C for 45 s, and 72°C for 60 s followed by one melt curve cycle of 65°C to 95°C with a temperature increment of 0.5°C for 5 s. The ramping rate was set to 2°C/s throughout the cycles with three technical replicates. Details of the primer sequence are described in Supplemental Data Set 4.

Statistical Analysis

The statistical analysis was performed using one-way ANOVA, followed by Dunnett's multiple comparisons test ($\alpha = 0.05$), to compare each sample against the wild-type control (Col-0). Data were expressed as mean ± SEM. Statistical significance was expressed as follows: ****$P \leq 0.0001$, ***$P \leq 0.001$, **$P \leq 0.01$, *$P \leq 0.05$ and nonsignificant (ns; $P > 0.05$). n denotes the number of samples. All analyses were done using GraphPad PRISM v.8.3.1.

Accession Numbers

Microarray data are available in the GEO database under accession number GSE130061.

Supplemental Data

Supplemental Figure 1. Aniline blue staining for sieve plates in the phloem SEs and SHR expression.

Supplemental Figure 2. Quantification and classification of phloem SE development and stele cell counting.

Supplemental Figure 3. *PHB* expression in the phloem pole suppresses the stele cell proliferation activity in *shr-2 phb-6*.

Supplemental Figure 4. SHR expression in the stele affects root growth.

Supplemental Figure 5. Expression dynamics of SHR-dependent phloem-enriched transcription factors in response to SHR induction.

Supplemental Figure 6. Characterization of *snd2* and *nars1* mutants.

Supplemental Figure 7. Comparisons of phloem development among the wild type, *snd2* and *nars1*.

Supplemental Figure 8. Expression patterns of *NARS1* and its effect on *SND2*.

Supplemental Figure 9. NARS1 regulates the most phloem-enriched TFs that are downstream of SHR.

Supplemental Figure 10. Promotion of cell divisions for phloem sieve element formation by *NARS1* and *SND2*.

Supplemental Figure 11. Analysis of companion cell development in transgenic plants ectopically expressing *NARS1* and *SND2*.

Supplemental Figure 12. Dissection of the SHR-NARS1-SND2 pathway.

Supplemental Data Set 1. ANOVA of the numbers of phloem SEs and stele cells scored in selected genotypes.

Supplemental Data Set 2. Normalized expression data in the root stele of wild type, *shr-2*, and *ProCRE1:SHRΔNLELDV-nlsGFP shr-2* (SHRΔNLELDV).

Supplemental Data Set 3. Phloem-enriched genes upregulated by SHR in the stele.

Supplemental Data Set 4. List of primers used in this study.

ACKNOWLEDGMENTS

We thank Nam Hoang for the proofreading of the article and for assisting with the statistics, Muhammad Kamran for the proofreading of the article, and Chulmin Park for assisting with the imaging steps. This work was supported by funding from the National Research Foundation of Korea (NRF; grants 2016R1A2B2015258 and 2018R1A5A1023599 to J.-Y. Lee), the Brain Korea 21 Plus Program (to H.K. and K.H.R.), and the WooDuk Foundation (to H.K.).

AUTHOR CONTRIBUTIONS

J.Z. and J.-Y.L. conceptualized, investigated, and analyzed data pertaining to the involvement of *SHR* in the phloem development process; H.K. and J.-Y.L. conceptualized, investigated, and analyzed data related to the involvement of *NARS1* and *SND2*; D.K., G.J., K.H.R., and J.S. contributed to the compilation of the data; S.M. and Y.H. contributed unpublished plant materials and data; J.Z., H.K., G.J., J.S., D.K., S.M., Y.H. and J.-Y.L. contributed to the writing of the article. All authors read and approved of the final article.

Received June 20, 2019; revised February 6, 2020; accepted February 25, 2020; published February 28, 2020.

REFERENCES

Abrash, E.B., and Bergmann, D.C. (2009). Asymmetric cell divisions: a view from plant development. Dev. Cell **16:** 783–796.

Baum, S.F., Dubrovsky, J.G., and Rost, T.L. (2002). Apical organization and maturation of the cortex and vascular cylinder in Arabidopsis thaliana (Brassicaceae) roots. Am. J. Bot. **89:** 908–920.

Berger, F., Haseloff, J., Schiefelbein, J., and Dolan, L. (1998). Positional information in root epidermis is defined during embryogenesis and acts in domains with strict boundaries. Curr. Biol. **8:** 421–430.

Birnbaum, K., Jung, J.W., Wang, J.Y., Lambert, G.M., Hirst, J.A., Galbraith, D.W., and Benfey, P.N. (2005). Cell type-specific expression profiling in plants via cell sorting of protoplasts from fluorescent reporter lines. Nat. Methods **2:** 615–619.

Blob, B., Heo, J.O., and Helariutta, Y. (2018). Phloem differentiation: An integrative model for cell specification. J. Plant Res. **131:** 31–36.

Bonke, M., Thitamadee, S., Mähönen, A.P., Hauser, M.-T., and Helariutta, Y. (2003). APL regulates vascular tissue identity in Arabidopsis. Nature **426:** 181–186.

Brady, S.M., Orlando, D.A., Lee, J.Y., Wang, J.Y., Koch, J., Dinneny, J.R., Mace, D., Ohler, U., and Benfey, P.N. (2007). A high-resolution root spatiotemporal map reveals dominant expression patterns. Science **318:** 801–806.

Carlsbecker, A., et al. (2010). Cell signalling by microRNA165/6 directs gene dose-dependent root cell fate. Nature **465:** 316–321.

Clough, S.J., and Bent, A.F. (1998). Floral dip: A simplified method for *Agrobacterium*-mediated transformation of *Arabidopsis thaliana*. Plant J. **16:** 735–743.

De Smet, I., and Beeckman, T. (2011). Asymmetric cell division in land plants and algae: The driving force for differentiation. Nat. Rev. Mol. Cell Biol. **12:** 177–188.

Furuta, K.M., et al. (2014). Plant development. Arabidopsis NAC45/86 direct sieve element morphogenesis culminating in enucleation. Science **345:** 933–937.

Gallagher, K.L., and Benfey, P.N. (2009). Both the conserved GRAS domain and nuclear localization are required for SHORT-ROOT movement. Plant J. **57:** 785–797.

Hayashi, H., Fukuda, A., Suzui, N., and Fujimaki, S. (2000). Proteins in the sieve element-companion cell complexes: Their detection, localization and possible functions. Aust. J. Plant Physiol. **27:** 489–496.

Helariutta, Y., Fukaki, H., Wysocka-Diller, J., Nakajima, K., Jung, J., Sena, G., Hauser, M.-T., and Benfey, P.N. (2000). The SHORT-ROOT gene controls radial patterning of the Arabidopsis root through radial signaling. Cell **101:** 555–567.

Heyer, L.J., Kruglyak, S., and Yooseph, S. (1999). Exploring expression data: Identification and analysis of coexpressed genes. Genome Res. **9:** 1106–1115.

Ingram, P., Dettmer, J., Helariutta, Y., and Malamy, J.E. (2011). Arabidopsis Lateral Root Development 3 is essential for early phloem development and function, and hence for normal root system development. Plant J. **68:** 455–467.

Irizarry, R.A., Hobbs, B., Collin, F., Beazer-Barclay, Y.D., Antonellis, K.J., Scherf, U., and Speed, T.P. (2003). Exploration, normalization, and summaries of high density oligonucleotide array probe level data. Biostatistics **4:** 249–264.

Kajala, K., Ramakrishna, P., Fisher, A., Bergmann, D.C., De Smet, I., Sozzani, R., Weijers, D., and Brady, S.M. (2014). Omics and modelling approaches for understanding regulation of asymmetric cell divisions in arabidopsis and other angiosperm plants. Ann. Bot. **113:** 1083–1105.

Kerszberg, M., and Wolpert, L. (2007). Specifying positional information in the embryo: Looking beyond morphogens. Cell **130:** 205–209.

Khan, J.A., Wang, Q., Sjölund, R.D., Schulz, A., and Thompson, G.A. (2007). An early nodulin-like protein accumulates in the sieve

element plasma membrane of Arabidopsis. Plant Physiol. **143:** 1576–1589.

Knoblauch, M., and van Bel, A.J.E. (1998). Sieve tubes in action. Plant Cell **10:** 35–50.

Kondo, Y., Nurani, A.M., Saito, C., Ichihashi, Y., Saito, M., Yamazaki, K., Mitsuda, N., Ohme-Takagi, M., and Fukuda, H. (2016). Vascular cell induction culture system using Arabidopsis leaves (VISUAL) reveals the sequential differentiation of sieve element-like cells. Plant Cell **28:** 1250–1262.

Kunieda, T., Mitsuda, N., Ohme-Takagi, M., Takeda, S., Aida, M., Tasaka, M., Kondo, M., Nishimura, M., and Hara-Nishimura, I. (2008). NAC family proteins NARS1/NAC2 and NARS2/NAM in the outer integument regulate embryogenesis in Arabidopsis. Plant Cell **20:** 2631–2642.

Lee, J.-Y., Colinas, J., Wang, J.Y., Mace, D., Ohler, U., and Benfey, P.N. (2006). Transcriptional and posttranscriptional regulation of transcription factor expression in Arabidopsis roots. Proc. Natl. Acad. Sci. USA **103:** 6055–6060.

Levesque, M.P., Vernoux, T., Busch, W., Cui, H., Wang, J.Y., Blilou, I., Hassan, H., Nakajima, K., Matsumoto, N., Lohmann, J.U., Scheres, B., and Benfey, P.N. (2006). Whole-genome analysis of the SHORT-ROOT developmental pathway in Arabidopsis. PLoS Biol. **4:** e143.

Lohaus, G., Winter, H., Riens, B., and Heldt, H.W. (1995). Further-studies of the phloem loading process in leaves of barley and spinach - the comparison of metabolite concentrations in the apoplastic compartment with those in the cytosolic compartment and in the sieve tubes. Bot. Acta **108:** 270–275.

Mähönen, A.P., Bonke, M., Kauppinen, L., Riikonen, M., Benfey, P.N., and Helariutta, Y. (2000). A novel two-component hybrid molecule regulates vascular morphogenesis of the Arabidopsis root. Genes Dev. **14:** 2938–2943.

Mähönen, A.P., Ten Tusscher, K., Siligato, R., Smetana, O., Díaz-Triviño, S., Salojärvi, J., Wachsman, G., Prasad, K., Heidstra, R., and Scheres, B. (2014). PLETHORA gradient formation mechanism separates auxin responses. Nature **515:** 125–129.

Mangan, S., and Alon, U. (2003). Structure and function of the feed-forward loop network motif. Proc. Natl. Acad. Sci. USA **100:** 11980–11985.

Marhava, P., Bassukas, A.E.L., Zourelidou, M., Kolb, M., Moret, B., Fastner, A., Schulze, W.X., Cattaneo, P., Hammes, U.Z., Schwechheimer, C., and Hardtke, C.S. (2018). A molecular rheostat adjusts auxin flux to promote root protophloem differentiation. Nature **558:** 297–300.

Miyashima, S., Koi, S., Hashimoto, T., and Nakajima, K. (2011). Non-cell-autonomous microRNA165 acts in a dose-dependent manner to regulate multiple differentiation status in the Arabidopsis root. Development **138:** 2303–2313.

Miyashima, S., et al. (2019). Mobile PEAR transcription factors integrate positional cues to prime cambial growth. Nature **565:** 490–494.

Nakajima, K., Sena, G., Nawy, T., and Benfey, P.N. (2001). Intercellular movement of the putative transcription factor SHR in root patterning. Nature **413:** 307–311.

Naouar, N., Vandepoele, K., Lammens, T., Casneuf, T., Zeller, G., van Hummelen, P., Weigel, D., Rätsch, G., Inzé, D., Kuiper, M., De Veylder, L., and Vuylsteke, M. (2009). Quantitative RNA expression analysis with Affymetrix Tiling 1.0R arrays identifies new E2F target genes. Plant J. **57:** 184–194.

Nawy, T., Lee, J.-Y., Colinas, J., Wang, J.Y., Thongrod, S.C., Malamy, J.E., Birnbaum, K., and Benfey, P.N. (2005). Transcriptional profile of the Arabidopsis root quiescent center. Plant Cell **17:** 1908–1925.

Oparka, K.J., and Turgeon, R. (1999). Sieve elements and companion cells-traffic control centers of the phloem. Plant Cell **11:** 739–750.

Paciorek, T., Sauer, M., Balla, J., Wiśniewska, J., and Friml, J. (2006). Immunocytochemical technique for protein localization in sections of plant tissues. Nat. Protoc. **1:** 104–107.

Rodriguez-Villalon, A., Gujas, B., Kang, Y.H., Breda, A.S., Cattaneo, P., Depuydt, S., and Hardtke, C.S. (2014). Molecular genetic framework for protophloem formation. Proc. Natl. Acad. Sci. USA **111:** 11551–11556.

Saeed, A.I., Bhagabati, N.K., Braisted, J.C., Liang, W., Sharov, V., Howe, E.A., Li, J., Thiagarajan, M., White, J.A., and Quackenbush, J. (2006). TM4 microarray software suite. Methods Enzymol. **411:** 134–193.

Sebastian, J., Ryu, K.H., Zhou, J., Tarkowská, D., Tarkowski, P., Cho, Y.H., Yoo, S.D., Kim, E.S., and Lee, J.Y. (2015). PHABULOSA controls the quiescent center-independent root meristem activities in Arabidopsis thaliana. PLoS Genet. **11:** e1004973.

Sena, G., Jung, J.W., and Benfey, P.N. (2004). A broad competence to respond to SHORT ROOT revealed by tissue-specific ectopic expression. Development **131:** 2817–2826.

Sjolund, R.D. (1997). The phloem sieve element: A river runs through it. Plant Cell **9:** 1137–1146.

Smyth, G.K. (2004). Linear models and empirical bayes methods for assessing differential expression in microarray experiments. Stat. Appl. Genet. Mol. Biol. **3:** Article3.

Stadler, R., and Sauer, N. (1996). The Arabidopsis thaliana AtSUC2 gene is specifically expressed in companion cells. Bot. Acta **109:** 299–306.

Taylor, S.C., Laperriere, G., and Germain, H. (2017). Droplet Digital PCR versus qPCR for gene expression analysis with low abundant targets: from variable nonsense to publication quality data. Sci. Rep. **7:** 2409.

Truernit, E., Bauby, H., Belcram, K., Barthélémy, J., and Palauqui, J.-C. (2012). OCTOPUS, a polarly localised membrane-associated protein, regulates phloem differentiation entry in Arabidopsis thaliana. Development **139:** 1306–1315.

Vatén, A., et al. (2011). Callose biosynthesis regulates symplastic trafficking during root development. Dev. Cell **21:** 1144–1155.

Wallner, E.S., et al. (2017). Strigolactone- and Karrikin-Independent SMXL proteins are central regulators of phloem formation. Curr. Biol. **27:** 1241–1247.

Zhong, R., Richardson, E.A., and Ye, Z.-H. (2007). The MYB46 transcription factor is a direct target of SND1 and regulates secondary wall biosynthesis in Arabidopsis. Plant Cell **19:** 2776–2792.